

Decreased Sirtuin Deacetylase Activity in *LRRK2* G2019S iPSC-Derived Dopaminergic Neurons

Andrew J. Schwab,^{1,3} Samantha L. Sison,¹ Michael R. Meade,¹ Katarzyna A. Broniowska,^{2,4} John A. Corbett,² and Allison D. Ebert^{1,*}

¹Department of Cell Biology, Neurobiology and Anatomy

²Department of Biochemistry

Medical College of Wisconsin, 8701 Watertown Plank Road, Milwaukee, WI 53226, USA

³Present address: U.S. Environmental Protection Agency, Durham, NC 27709, USA

⁴Present address: Metabolon, Inc. Morrisville, NC 27560, USA

*Correspondence: aebert@mcw.edu

<https://doi.org/10.1016/j.stemcr.2017.10.010>

SUMMARY

Mitochondrial changes have long been implicated in the pathogenesis of Parkinson's disease (PD). The glycine to serine mutation (G2019S) in leucine-rich repeat kinase 2 (*LRRK2*) is the most common genetic cause for PD and has been shown to impair mitochondrial function and morphology in multiple model systems. We analyzed mitochondrial function in *LRRK2* G2019S induced pluripotent stem cell (iPSC)-derived neurons to determine whether the G2019S mutation elicits similar mitochondrial deficits among central and peripheral nervous system neuron subtypes. *LRRK2* G2019S iPSC-derived dopaminergic neuron cultures displayed unique abnormalities in mitochondrial distribution and trafficking, which corresponded to reduced sirtuin deacetylase activity and nicotinamide adenine dinucleotide levels despite increased sirtuin levels. These data indicate that mitochondrial deficits in the context of *LRRK2* G2019S are not a global phenomenon and point to distinct sirtuin and bioenergetic deficiencies intrinsic to dopaminergic neurons, which may underlie dopaminergic neuron loss in PD.

INTRODUCTION

Mutations in leucine-rich repeat kinase 2 (*LRRK2*) are associated with both familial and sporadic Parkinson's disease (PD), and exhibit clinical symptoms and pathology typical of sporadic PD (Gatto et al., 2013). The G2019S mutation is the most common and confers hyper-kinase activity, but it is unclear how the gain of function in kinase activity results in PD pathogenesis. The precise biological function of *LRRK2* remains largely unknown, but increasing evidence suggests that mutations in *LRRK2* contribute to mitochondrial dysfunction and oxidative stress (Wang et al., 2008; Ng et al., 2009; Saha et al., 2009; Mortiboys et al., 2010).

In vivo and *in vitro* studies examining the consequence of *LRRK2* G2019S on mitochondrial health show altered mitochondrial morphology, increased fragmentation, elevated reactive oxygen species (ROS) production, and decreased respiration (Ryan et al., 2015; Yue et al., 2015). Induced pluripotent stem cell (iPSC) derived neurons generated from homozygous and heterozygous *LRRK2* G2019S patients showed mitochondrial damage (Sanders et al., 2014), deficits in basal and maximal respiration, an increase in mitochondrial trafficking (Cooper et al., 2012), and increased susceptibility to H₂O₂, 6-OHDA, and rotenone (Nguyen et al., 2011; Reinhardt et al., 2013). Factors implicated in dopaminergic vulnerability include higher metabolic activity, increased oxidative stress due to dopamine oxidation, and calcium buffering defects, all of which may converge on mitochondrial malfunction.

We used *LRRK2* G2019S iPSC-derived dopaminergic, glutamatergic, and sensory neurons to explore functionally relevant mitochondrial parameters by which neurons may be susceptible to disease. We focused on addressing two key questions. First, we asked if the *LRRK2* G2019S mutation causes consistent mitochondrial changes across multiple neuronal subtypes. We found that mitochondrial respiration deficits were observed in *LRRK2* G2019S iPSC-derived dopaminergic and glutamatergic neuron cultures, whereas no mitochondrial defects were observed in *LRRK2* G2019S iPSC-derived peripheral sensory neuron cultures, suggesting a shared CNS weakness. However, *LRRK2* G2019S iPSC-derived dopaminergic neurons displayed additional mitochondrial distribution and trafficking abnormalities, indicating a unique midbrain dopaminergic phenotype. Second, we asked what cellular mechanisms may contribute to the unique mitochondrial phenotypes observed in dopaminergic neuron cultures. Accumulating evidence suggests that protein acetylation is a key regulatory mechanism in mitochondrial function. Sirtuins are protein lysine deacetylases that are localized to the nucleus, cytosol, and mitochondria, where they serve a variety of anti-aging and metabolic roles (Chalkiadaki and Guarente, 2012; Guarente, 2013; Herskovits and Guarente, 2013; Buler et al., 2016). Humans encode seven distinct sirtuins that harbor various roles in mitochondrial biogenesis, movement, and energetics, and collectively may play a role in the defects observed in PD dopaminergic neurons. Surprisingly, we found that



LRRK2 G2019S iPSC-derived dopaminergic neurons exhibit increased sirtuin levels, but decreased deacetylase activity compared with control cells. Because sirtuins require nicotinamide adenine dinucleotide (NAD⁺) as a co-substrate to catalyze deacetylation, we assessed NAD⁺ levels and observed a decreased NAD⁺ pool in *LRRK2* G2019S dopaminergic neurons compared with healthy dopaminergic neurons. The decrease in NAD⁺ correlated with elevated acetylation of sirtuin substrates p53, α -tubulin, and SOD2. Together, these data suggest that *LRRK2* G2019S confers cell-type specific bioenergetic defects, and that dopaminergic neurons may be more significantly impacted in PD due to low endogenous NAD⁺ levels and reduced sirtuin deacetylase activity.

RESULTS

LRRK2 G2019S iPSC-Derived Dopaminergic Neurons Display Altered Mitochondrial Content and Distribution

To examine mitochondrial health across neuronal subtypes expressing the *LRRK2* G2019S mutation, we utilized human iPSCs derived from three independent *LRRK2* G2019S patients and three unaffected control individuals (Schwab and Ebert, 2015) and differentiated the cells toward midbrain dopaminergic neurons, forebrain glutamatergic neurons, and peripheral sensory neurons. Importantly, we have previously shown that neurons from these *LRRK2* G2019S iPSC lines have consistently elevated expression of phosphorylated LRRK2 at serine 935, but similar levels of total LRRK2 protein compared with the control iPSC neurons (Schwab and Ebert, 2015).

We first examined overall mitochondrial content and distribution across the three neuronal subtypes. Cells were immunostained for the mitochondrial membrane protein TOM20 and co-labeled with tyrosine hydroxylase (TH), β III-tubulin (TUJ1), or peripherin to mark dopaminergic, glutamatergic, and sensory neurons, respectively (Figures 1A, 1D, 1G, and S1A). Immunofluorescence (Figure S1B) and western blot analysis (Figure S1C) for the NMDA receptor 2B subunit (NR2B) were used to further confirm glutamatergic neuron identity. Consistent with our previous report (Schwab and Ebert, 2015), there was no difference in differentiation efficiency across the individual cell lines (Figures 1B, 1E, and 1H), and differentiation efficiencies were consistent with other reports in the literature (Chambers et al., 2009, 2012; Kriks et al., 2011). Using immunofluorescence intensity (Figures 1C, 1F, and 1I) and western blot analysis (Figure 1J), mitochondrial content was reduced in *LRRK2* G2019S iPSC-derived dopaminergic neurons compared with controls, but not in the other neuronal subtypes. We next measured mitochondrial distribution

along the neurite and divided the data points into four equal quartiles to assess differences in proximal versus distal distribution. Because we and others have shown that *LRRK2* G2019S iPSC-derived dopaminergic neurons exhibit shortened neurites (Cooper et al., 2012; Sanchez-Danes et al., 2012; Reinhardt et al., 2013; Schwab and Ebert, 2015), quartiles were determined relative to each neuronal subtype and not compared across neuron types. *LRRK2* G2019S iPSC-derived dopaminergic neurons displayed significantly reduced mitochondrial distribution along the distal neurite length (Figure 1K). In contrast to previous reports using mouse cortical neurons expressing *LRRK2* G2019S (Cherra et al., 2013), neither mitochondrial content nor distribution was diminished in *LRRK2* G2019S glutamatergic and sensory neurons compared with control neurons (Figures 1F, 1I, 1L, and 1M), suggesting neuron specific mitochondrial properties in human *LRRK2* G2019S conditions.

LRRK2 G2019S iPSC-Derived Dopaminergic Neurons Display Increased Mitochondrial Velocity and Motility

Neurons depend on regulated mitochondrial trafficking to match energy demand and to control the clearance of damaged mitochondria (Ashrafi and Schwarz, 2013). We utilized live-cell imaging to investigate if *LRRK2* G2019S induced changes in mitochondrial trafficking and mobility within iPSC-derived dopaminergic, glutamatergic, and sensory neurons. We observed an increase in mitochondrial velocity in *LRRK2* G2019S iPSC-derived dopaminergic neurons compared with control dopaminergic neurons (Figure 2A). Interestingly, neither *LRRK2* G2019S glutamatergic nor sensory neurons were altered compared with their respective control neurons (Figure 2A). Similar to a previous study (Cooper et al., 2012), we also saw an increase in the percentage of mobile mitochondria in dopaminergic neurons, but this effect was not observed in *LRRK2* G2019S glutamatergic or sensory neurons (Figure 2B). Finally, we found that *LRRK2* G2019S iPSC-derived dopaminergic neurons display increased retrograde mitochondrial velocity (Figure 2C), which correlates with diminished mitochondrial content in the distal neurite (Figure 1K). Together, these data highlight intrinsic dopaminergic neuron mitochondrial trafficking deficits.

Mitochondrial Respiration Is Decreased in *LRRK2* G2019S iPSC-Derived Dopaminergic and Glutamatergic Neurons

We next asked if mitochondrial bioenergetics was affected in *LRRK2* G2019S iPSC-derived neurons. Control and *LRRK2* G2019S iPSCs were differentiated into dopaminergic, glutamatergic, and sensory neurons to measure oxygen consumption rate (OCR) (Dranka et al., 2011; Zhang et al., 2012; Patitucci and Ebert, 2016). Basal glycolytic rates

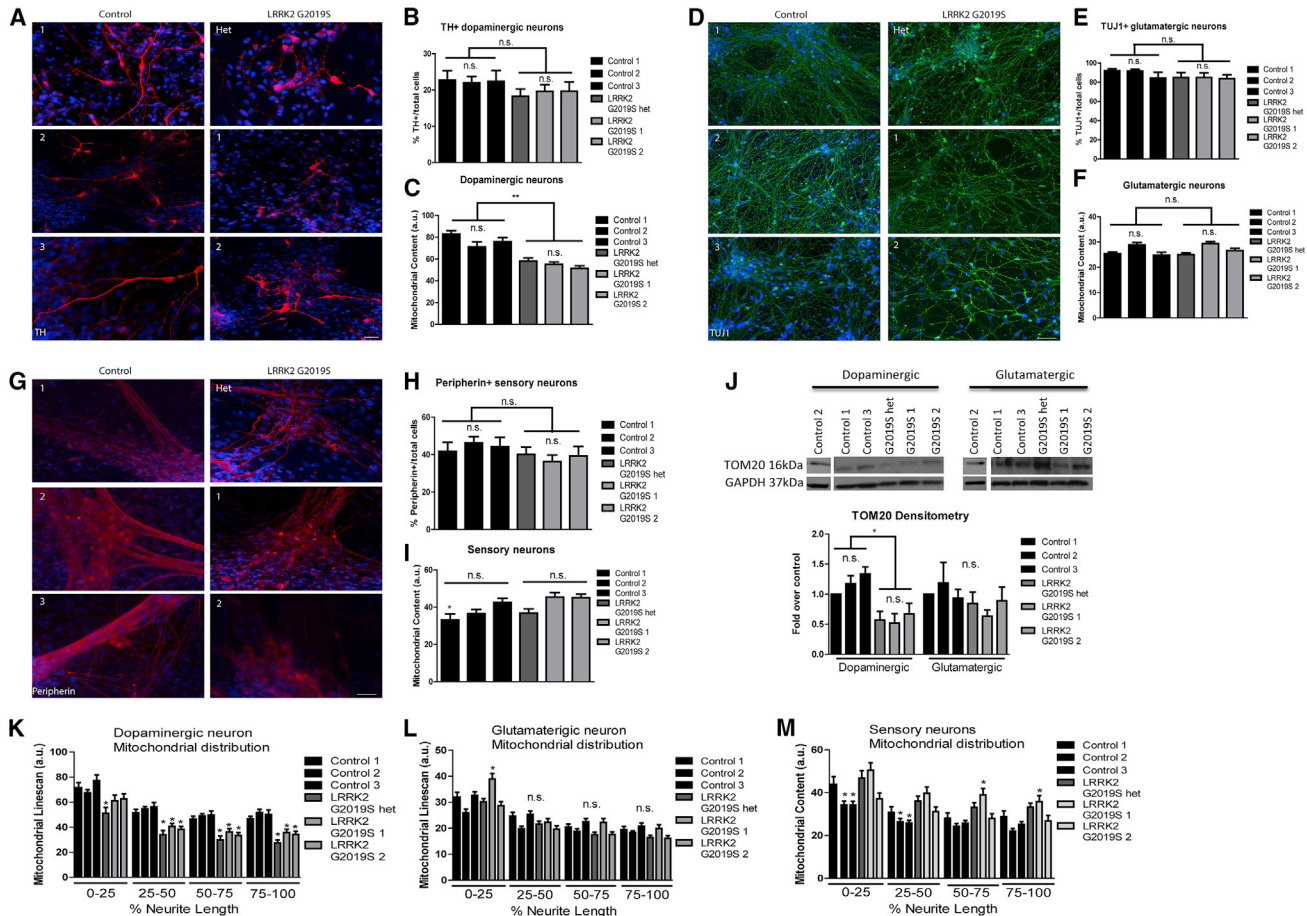


Figure 1. *LRRK2* G2019S iPSC-Derived Dopaminergic Neurons Display Altered Mitochondrial Content and Distribution

Representative images of each individual control line (1, 2, and 3) and each individual *LRRK2* G2019S iPSC line (het, 1, and 2) immunostained for (A) tyrosine hydroxylase (TH, red), (D) β III-tubulin (TUJ1, green), and (G) peripherin (red) to mark dopaminergic, glutamatergic, and sensory neurons, respectively. Nuclei labeled with Hoechst (blue). Scale bars, 50 μ m. Quantification of differentiation efficiency (B, E, and H), mitochondrial content (C, F, and I), TOM20 protein (J), and mitochondrial distribution (K, L, and M) compared by one-way repeated measures ANOVA with Tukey's *post-hoc* test. n.s., not significant. ** $p < 0.01$ in (C) indicates that all three *LRRK2* samples are significantly reduced compared with all three control samples. * $p < 0.05$ in (I) indicates that control 1 is significantly reduced compared with *LRRK2* 1 and 2. * $p < 0.05$ in (J) indicates that all three *LRRK2* samples are significantly reduced compared with all three control samples. * $p < 0.05$ in (K) indicates that *LRRK2* het is different from all three controls (0%–25%) and all three *LRRK2* lines are different from all three control lines for 25%–50%, 50%–75%, and 75%–100%. * $p < 0.05$ in (L) indicates that *LRRK2* 1 is significantly different from all samples at 0%–25%. * $p < 0.05$ in (M) indicates that control 2 and 3 are different from *LRRK2* het and *LRRK2* 1 at 0%–25% and 25%–50%, and that *LRRK2* 1 is different from all three controls at 50%–75% and 75%–100%. $n = 4$ independent experiments. All error bars are SEM. See also Figure S1.

were not changed in any of the *LRRK2* G2019S neurons compared with controls (data not shown). However, consistent with previous studies (Mortiboys et al., 2010, 2015; Cooper et al., 2012; Papkovskaia et al., 2012), we observed a marked decrease in OCR for ATP-linked (Figure 3A), maximal (Figure 3B), and spare respiration (Figure 3C) in *LRRK2* G2019S dopaminergic neuron cultures compared with control dopaminergic neuron cultures. Interestingly, we also observed a decrease in these same parameters for *LRRK2* G2019S forebrain glutamatergic neuron cultures

compared with control, but not in *LRRK2* G2019S sensory neuron cultures (Figures 3A–3C). Together, these data suggest that *LRRK2* G2019S may preferentially alter mitochondrial respiration rates of central neurons and spare peripheral neurons.

Consistent with the observed decrease in bioenergetics, *LRRK2* G2019S dopaminergic cultures displayed diminished ATP and ADP levels compared with control neurons, whereas *LRRK2* G2019S glutamatergic cultures displayed changes only in ATP levels (Figures S2A and S2B). No change

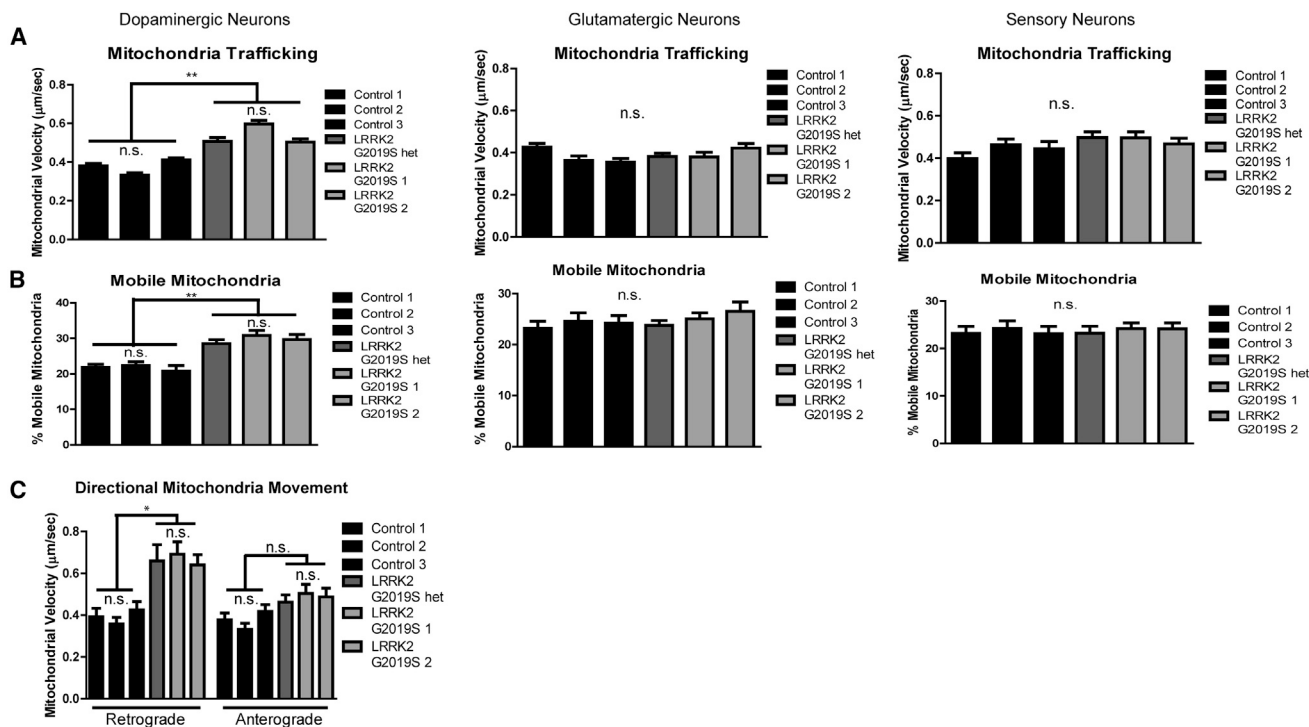


Figure 2. *LRRK2* G2019S iPSC-Derived Dopaminergic Neurons Display Increased Mitochondrial Velocity and Motility

Measurements of (A) mitochondrial velocity ($\mu\text{m}/\text{s}$), (B) percent mobile mitochondria, and (C) direction of mitochondrial movement are shown for each individual iPSC line. There was a significant difference for each of the three *LRRK2* lines compared with each of the control lines in the dopaminergic neuron cultures, but not in either the glutamatergic or sensory neuron cultures. n.s., not significant. * $p < 0.05$ and ** $p < 0.01$ by one-way repeated measures ANOVA with Tukey's *post-hoc* test. $n = 4$ independent experiments. All error bars are SEM. See also Figure S4.

was observed in sensory neuron cultures (Figures S2A and S2B). To further assess the reduction in ATP levels, we examined components of the electron transport chain by western blot using the OXPHOS antibody cocktail. Complex I (NDUFB8) and IV (COX II) were undetectable in all neuron cultures, and complex V (ATP5A) and II (SDHB) levels were unchanged (Figures S3A–S3C). However, the levels of complex III (UQCRC2) were significantly decreased in both dopaminergic and glutamatergic neuron cultures from *LRRK2* G2019S iPSCs compared with control (Figures S3D and S3E). Therefore, it is possible that decreased expression or increased degradation of complex III in *LRRK2* G2019S iPSC-derived dopaminergic and glutamatergic neuron cultures alters proton transport, thereby diminishing the proton gradient necessary for ATP production.

LRRK2 Kinase Inhibition Using GSK2578215A Does Not Restore Mitochondrial Dysfunction

Since the G2019S mutation confers hyper-kinase activity (West et al., 2005; Greggio et al., 2006; Jaleel et al., 2007; Luzon-Toro et al., 2007), we tested whether *LRRK2* kinase inhibition using GSK2578215A (Reith et al., 2012) could rescue

the observed mitochondrial defects in *LRRK2* G2019S iPSC-derived neurons. We have previously shown that treatment with 1 μM GSK2578215A reduced expression of phosphorylated *LRRK2* in *LRRK2* G2019S iPSC-derived neurons (Schwab and Ebert, 2015). Therefore, we treated dopaminergic, glutamatergic, and sensory neuron cultures with GSK2578215A (1 μM) for 1 week prior to endpoint analysis. However, *LRRK2* kinase inhibition only showed an effect in the *LRRK2* G2019S Het line for mitochondrial velocity, but there was no effect in any *LRRK2* G2019S line for ATP-linked, maximal, and spare respiration in dopaminergic neurons. GSK2578215A did not have a positive or negative effect on glutamatergic and sensory neurons (Figures S4A and S4B). These results suggest that increased kinase activity is not directly contributing to mitochondrial malfunction in this model system.

LRRK2 G2019S Dopaminergic Neuron Cultures Show Increased Sirtuin Expression but Decreased Deacetylase Activity

Sirtuins are a family of NAD^+ -dependent protein deacetylases that regulate many cellular processes, and changes

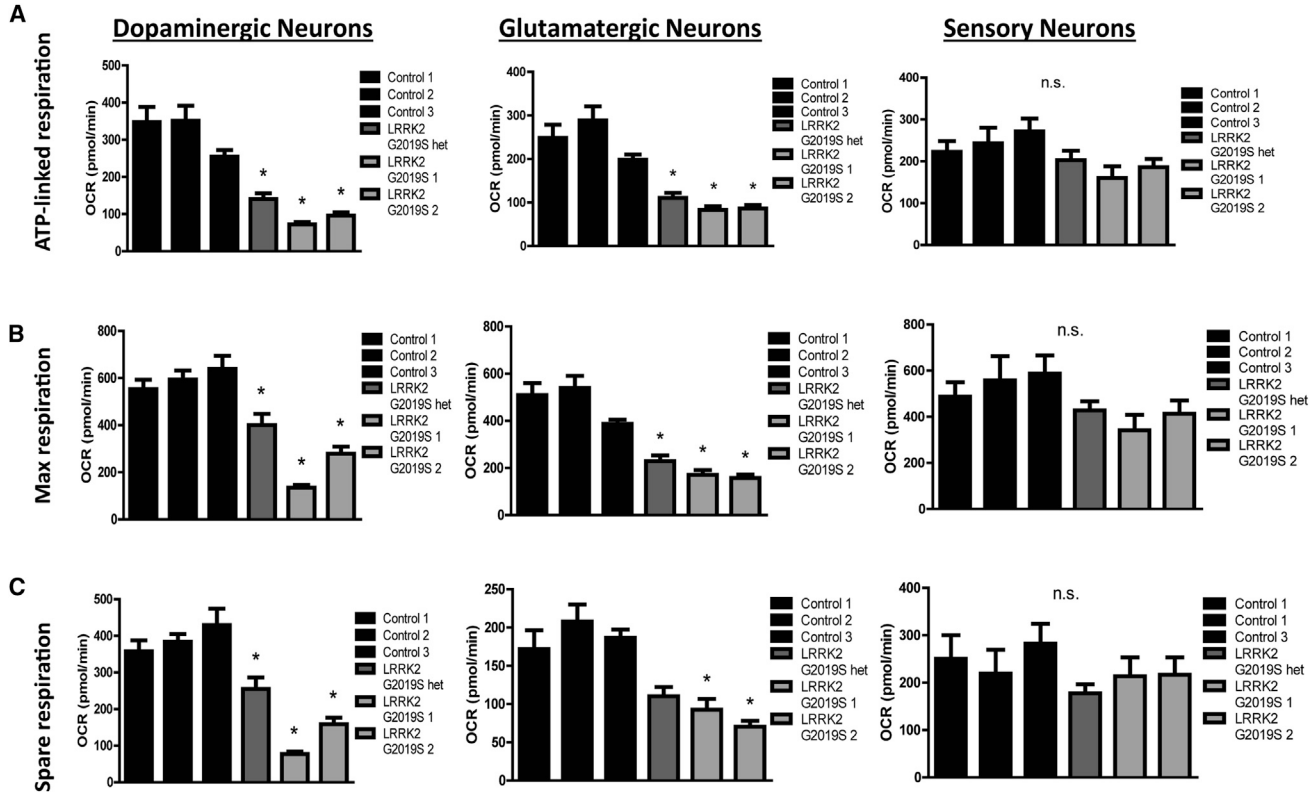


Figure 3. Mitochondrial Respiration Is Decreased in *LRRK2* G2019S iPSC-Derived Dopaminergic and Glutamatergic Cultures

All three *LRRK2* G2019S iPSC-derived dopaminergic and glutamatergic cultures display diminished (A) ATP-linked, (B) maximal, and (C) spare respiration compared with all three of the respective control cultures. *LRRK2* G2019S iPSC-derived sensory neurons are unchanged compared with controls. * $p < 0.05$ by one-way repeated measures ANOVA with Tukey's *post-hoc* test. $n = 4$ independent experiments. All error bars are SEM. See also Figures S2, S3, and S4.

in sirtuin expression levels may contribute to altered mitochondrial production, metabolism, and movement (Chalkiadaki and Guarente, 2012; Guarente, 2013; Herskovits and Guarente, 2013). Sirtuin-1 (SIRT1) has been shown to localize to the cytoplasm and nucleus where it plays a role in mitochondrial biogenesis (Tang, 2017). Western blot analysis of SIRT1 revealed a significant increase in *LRRK2* G2019S iPSC-derived dopaminergic neurons compared with control cells in which SIRT1 levels were below the detection limit (Figures 4A and 4B). SIRT1 deacetylates and activates PGC1 α (Rodgers et al., 2005; Liu et al., 2008; Canto et al., 2009; Wilson et al., 2010), which is an essential metabolic regulatory transcription factor. As expected based on the decreases in mitochondrial respiration and ATP pool, the levels of PGC1 α were markedly decreased in iPSC-derived *LRRK2* G2019S dopaminergic cultures (Figures 4C and 4D). In contrast, there was no difference in SIRT1 or PGC1 α expression in *LRRK2* G2019S glutamatergic cultures compared with control cultures (Figures S5A–S5C). Acetylated p53 is a known direct target of SIRT1 and showed a trend toward increased expression

in *LRRK2* G2019S iPSC-derived dopaminergic neurons compared with controls (Figures 4E and 4F), indicating reduced SIRT1 activity.

Sirtuin-2 (SIRT2) is known to mediate microtubule-based cellular trafficking through its effect on tubulin acetylation (North et al., 2003). Considering the significant alterations in mitochondrial movement in *LRRK2* G2019S iPSC-derived dopaminergic neurons (Figure 2), we tested whether SIRT2 expression and/or activity were likewise disrupted. Similar to SIRT1, SIRT2 protein levels were significantly increased in *LRRK2* G2019S iPSC-derived dopaminergic neurons compared with control (Figures 5A and 5B), but deacetylase activity was impaired as noted by the significant increase in the levels of acetylated α -tubulin (Figures 5A and 5C).

Next, we tested sirtuin-3 (SIRT3) levels and activity as SIRT3 is the primary mitochondrial deacetylase shown to regulate mitochondrial bioenergetics and ATP generation (Weir et al., 2013). Immunoblot analysis of SIRT3 expression levels revealed significantly increased expression in *LRRK2* G2019S dopaminergic cultures compared with

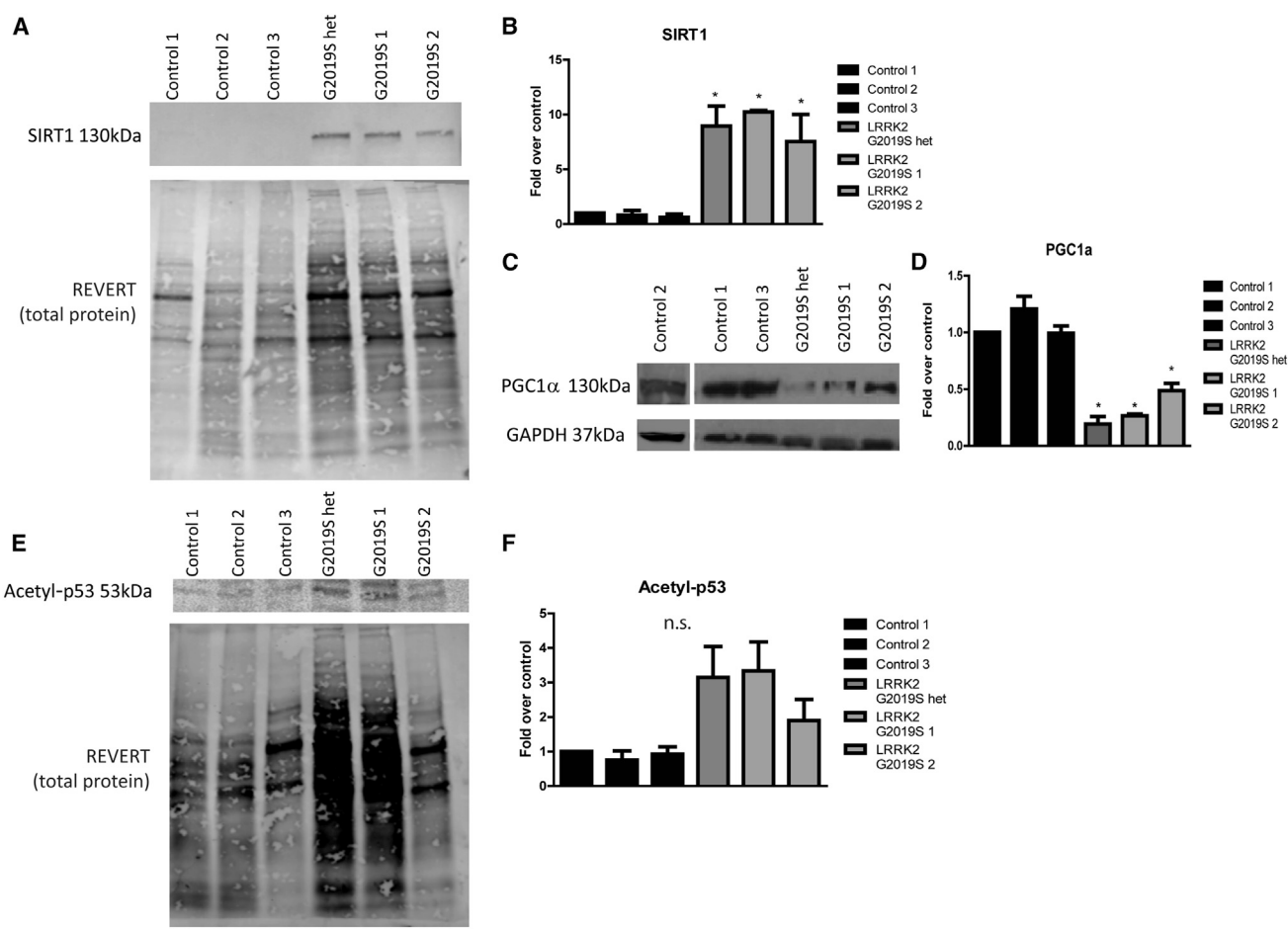


Figure 4. *LRRK2* G2019S Dopaminergic Neuron Cultures Show Altered Levels of Sirtuin-1, PGC1 α , and Acetylated p53

(A and B) Western blot analysis revealed a significant increase in (A and B) SIRT1 in all three *LRRK2* G2019S iPSC-derived dopaminergic cultures compared with the three controls. REVERT was used as a loading control.

(C and D) In contrast, PGC1 α expression levels were significantly reduced in all three *LRRK2* G2019S iPSC-derived dopaminergic cultures compared with controls. Glyceraldehyde-3-phosphate dehydrogenase (GAPDH) was used as a loading control.

(E and F) Levels of acetylated-p53 were increased in *LRRK2* G2019S iPSC-derived dopaminergic cultures, although this did not reach significance. REVERT was used as a loading control.

n.s., not significant. * $p < 0.05$ by one-way ANOVA with Tukey's *post-hoc* test. $n = 3$ independent experiments. All error bars are SEM. See also Figure S5.

control (Figures 6A and 6B). There was a trend toward a decrease in SIRT3 activity based on higher levels of acetylated SOD2 (Figures 6C and 6D). Although the changes associated with SOD2 did not reach significance, the trend is consistent with an overall diminished deacetylase activity in PD dopaminergic neurons. There was no difference in SIRT3 levels between control and *LRRK2* G2019S glutamatergic neurons (Figure S6). To determine whether increased SIRT levels were associated with excessive kinase activity, we tested whether GSK2578215A was sufficient to lower SIRT levels. However, similar to a lack of effect on mitochondrial dysfunction, we did not observe changes in SIRT1, SIRT2, or SIRT3 expression levels (data not shown).

Since sirtuins require NAD⁺ as a co-substrate to catalyze deacetylation, we hypothesized that low sirtuin activity in *LRRK2* G2019S iPSC-derived dopaminergic neurons was due to low NAD⁺ levels. Indeed, NAD⁺ levels were significantly decreased in *LRRK2* G2019S dopaminergic neurons compared with controls, a deficiency that was not observed in the other neuronal subtypes (Figure 7). Taken together, these data suggest that diminished NAD⁺ levels limit sirtuin deacetylase activity in *LRRK2* G2019S iPSC-derived dopaminergic neurons, and may underlie the mitochondrial malfunction observed in this system and contribute to selective dopaminergic neuron loss in PD.

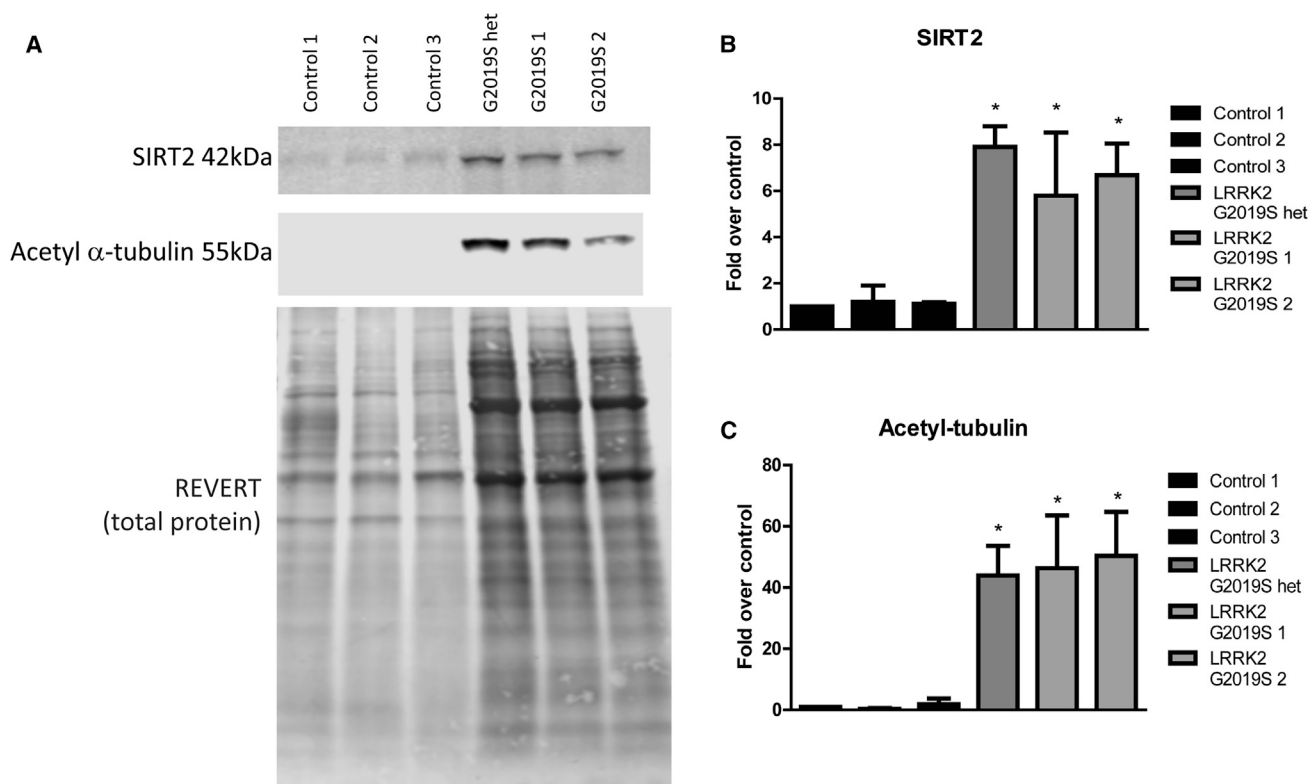


Figure 5. *LRRK2* G2019S Dopaminergic Neuron Cultures Show Increased Sirtuin-2 and Acetylated Tubulin

Western blot analysis revealed a significant increase in (A and B) SIRT2 and (A and C) acetylated tubulin expression in all three *LRRK2* G2019S iPSC-derived dopaminergic cultures compared with controls. REVERT was used as a loading control for both targets. * $p < 0.05$ by one-way ANOVA with Tukey's *post-hoc* test. $n = 3$ independent experiments. All error bars are SEM.

DISCUSSION

Evidence from *in vitro* and *in vivo* studies suggest that mitochondrial malfunction is a common characteristic in PD. Consistent with these reports, we show that *LRRK2* G2019S iPSC-derived neurons display mitochondrial abnormalities, including altered content, distribution, trafficking, and respiration, which appear to be independent of increased kinase activity; interestingly, these mitochondrial defects manifest differently depending upon neuron subtype, with dopaminergic neuron cultures exhibiting the most profound changes compared with glutamatergic or sensory neuron cultures.

Regulation of mitochondrial distribution is essential to meet metabolic requirements and to remove aged and damaged mitochondria. The decreased content and reduced distal distribution of mitochondria within dopaminergic neurons may be due to damaged mitochondria being removed by autophagy or an inability to sufficiently replenish the neurites with healthy mitochondria, which has been reported for *LRRK2* G2019S expressing mouse cortical neurons and SH-SY5Y cells (Cherra et al., 2013).

This result is in contrast to our data for *LRRK2* G2019S iPSC-derived glutamatergic neuron cultures. The discrepancy may be due to inherent differences between the model systems. In addition, the default forebrain telencephalic neuron patterning utilized here (Ebert et al., 2013; Kim et al., 2014) may not fully recapitulate the maturity and cell-type specificity found within the mouse cortex. Additional studies using specific iPSC cortical patterning techniques may be necessary to address the discrepancy (Mariani et al., 2012; Shi et al., 2012).

The distribution of mitochondria within neurons is dependent on efficient and regulated mitochondrial trafficking. The transport and function of mitochondria are linked as mitochondria supply ATP energy to motor proteins to transport them along the cytoskeleton to areas of high energy demand (Schwarz, 2013). Thus, abnormalities in mitochondrial trafficking may lead to abnormal mitochondrial distribution and protein transport and ultimately result in cellular dysfunction. We show that *LRRK2* G2019S can affect mitochondrial trafficking based on increased retrograde mitochondrial velocity and mobile mitochondria in *LRRK2* G2019S iPSC-derived

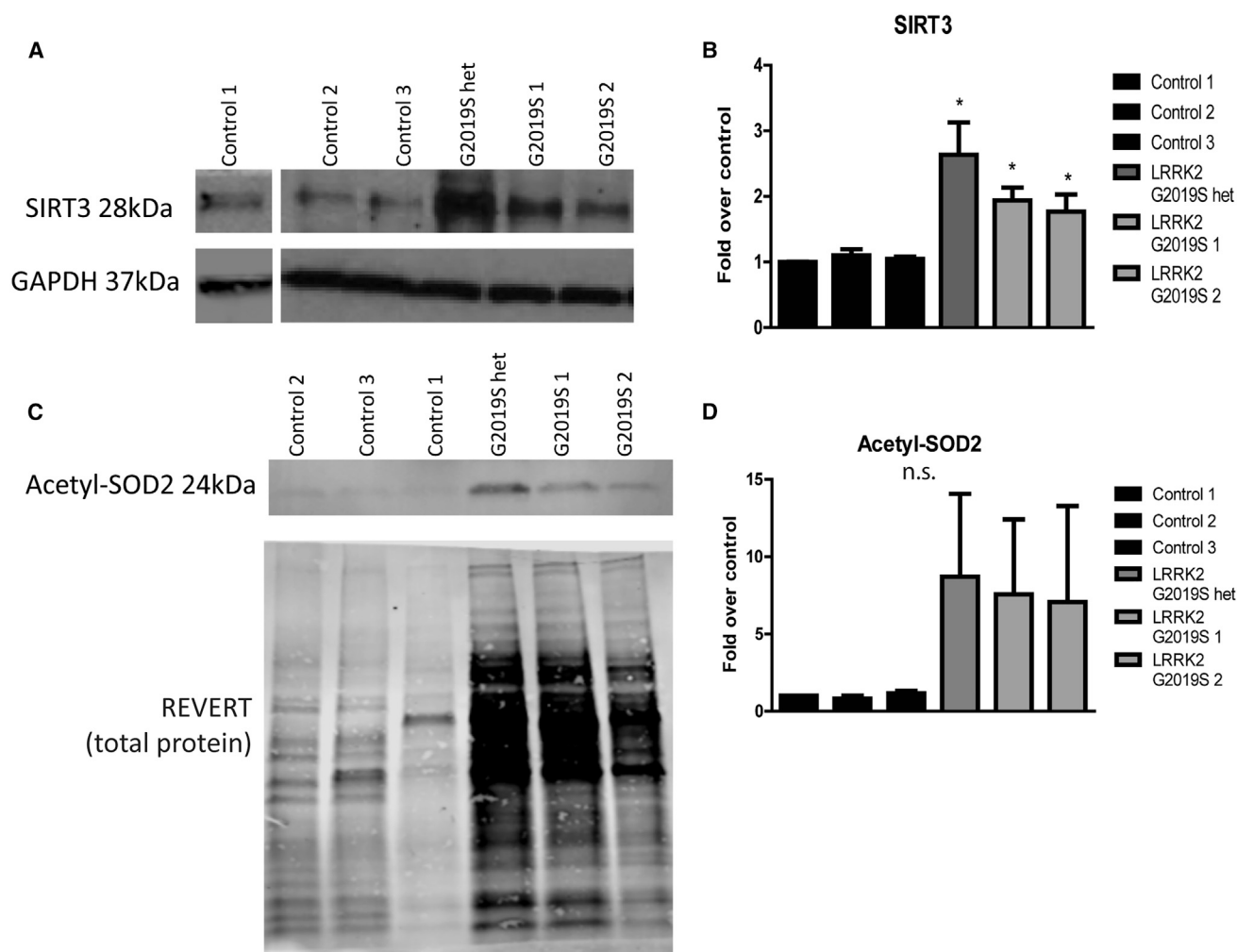


Figure 6. *LRRK2* G2019S Dopaminergic Neuron Cultures Show Increased Sirtuin-3 and Acetylated SOD2

Western blot analysis revealed a significant increase in (A and B) SIRT3 expression and (C and D) a trend toward increased acetylated SOD2 expression in *LRRK2* G2019S iPSC-derived dopaminergic cultures compared with control. SIRT3 was normalized to GAPDH, and SOD2 was normalized to REVERT. n.s., not significant. * $p < 0.05$ by one-way ANOVA with Tukey's *post-hoc* test. $n = 3$ independent experiments. All error bars are SEM. See also Figure S6.

dopaminergic neurons. These data correlate well with diminished mitochondrial content in the distal neurite. The trafficking results presented here are in contrast to a study using PD sporadic mitochondrial NT2 cybrids that showed a decline in overall mitochondrial velocity and a decrease in the percent mobile mitochondria (Esteves et al., 2014), but do support the findings in SH-SY5Y cultures (Cronin-Furman et al., 2013), and in *LRRK2* G2019S and PINK1 Q456X expressing neurons (Cooper et al., 2012). The increase in percent mobile mitochondria within *LRRK2* G2019S dopaminergic neurons suggests that the balance between motile and stationary mitochondria is perturbed. Anchored mitochondria provide local energy sources within neurons and are crucial to ensure that meta-

bolically active areas are supplied with ATP, especially at presynaptic terminals. Moreover, stationary mitochondria are also required for axonal branching and maintenance (Kang et al., 2008). Therefore, disruption in stationary mitochondria may explain the deficient neurite elongation and branching that we and others have observed in *LRRK2* G2019S-expressing neurons (MacLeod et al., 2006; Plowey et al., 2008; Cherra et al., 2010; Ramonet et al., 2011; Cooper et al., 2012; Sanchez-Danes et al., 2012; Reinhardt et al., 2013; Schwab and Ebert, 2015). However, additional studies are needed to establish a specific link between *LRRK2* G2019S and mitochondrial motility.

The *LRRK2* kinase inhibition results suggest that increased kinase activity due to the G2019S *LRRK2* mutation

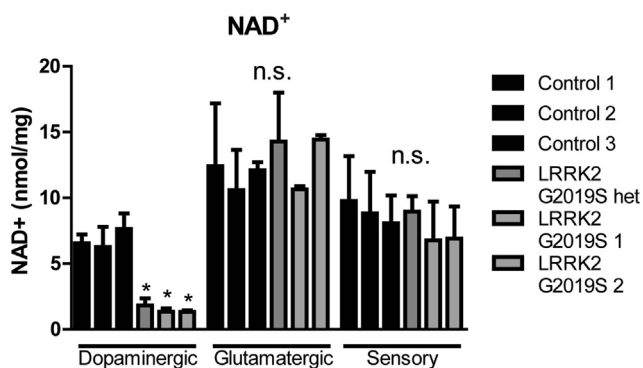


Figure 7. *LRRK2* G2019S Dopaminergic Neurons Exhibit Significantly Reduced NAD⁺ Levels

HPLC analysis revealed that all three *LRRK2* G2019S expressing dopaminergic neurons have significantly reduced NAD⁺ levels compared with controls. There was no difference between control and *LRRK2* G2019S-expressing neurons for either glutamatergic or sensory neuron cultures. n.s., not significant. * $p < 0.05$ compared with control dopaminergic neurons by one-way repeated measures ANOVA with Tukey's *post-hoc* test. $n = 3$ independent experiments. All error bars are SEM.

is not directly contributing to the mitochondrial and SIRT abnormalities in this iPSC-based system. Although GSK2578245A has been shown to be selective for *LRRK2* kinase inhibition (Reith et al., 2012), and we previously observed beneficial effects on morphology and calcium response in *LRRK2* G2019S iPSC-derived sensory neurons (Schwab and Ebert, 2015), it is possible that a different kinase inhibitor or treatment paradigm would be more effective.

A number of studies have tested the effect of modifying SIRT1, SIRT2, or SIRT3 in PD models, but the results have been mixed. For example, increasing levels of SIRT1 or SIRT3 protect dopaminergic neurons from toxin-induced cell death (Tang, 2017). In contrast, most data indicate that inhibiting SIRT2 expression is neuroprotective in PD models (Outeiro et al., 2007; Godena et al., 2014; Liu et al., 2014; Chen et al., 2015; Di Fruscia et al., 2015), although another study suggested otherwise (Patel and Chu, 2014). More research is needed to determine the specific contributions of the various sirtuins to PD, but the divergent effects of sirtuin upregulation and inhibition may be due to the different targets of the individual sirtuins. Importantly, previous studies have not examined the levels of NAD⁺ necessary for sirtuin activity in human dopaminergic neurons.

Recent studies have shown that PGC1 α and SIRT1 play key roles in cell metabolism and mitochondrial biogenesis (Rodgers et al., 2005; Revollo and Li, 2013). PGC1 α is active in the deacetylated form, which is achieved by the deacetylase function of SIRT1, and plays a protective role in ROS

defense. Here we show lower expression levels of active PGC1 α in *LRRK2* G2019S iPSC-derived dopaminergic neuron cultures compared with glutamatergic neuron cultures. We also found a strong trend toward increased acetylated p53 (~2- to 3-fold) in *LRRK2* G2019S iPSC-derived dopaminergic neurons compared with controls, a direct target of SIRT1, which may contribute to the vulnerability of dopaminergic neurons to oxidative stress in PD. To support this idea, acetylation of p53 at Lys382, the residue recognized by the antibody used here, is directly associated with activation of apoptosis and ROS production (Yamaguchi et al., 2009). Similarly, a small-molecule activator of PGC1 α resulted in enhanced resistance against oxidative stress in human dopaminergic neurons (Makela et al., 2016).

SIRT2 is localized to the cytoplasm and, together with HDAC6, is largely responsible for deacetylation of α -tubulin (North et al., 2003). Studies have shown that increasing acetylated α -tubulin, through inhibition of HDAC6, increases mitochondrial movement in hippocampal neurons (Chen et al., 2010). Our studies are consistent with this notion as we find significantly increased mitochondrial velocity and retrograde trafficking in the *LRRK2* G2019S iPSC-derived dopaminergic neurons. Mutant *LRRK2* has been shown to associate with deacetylated tubulin and disrupt vesicle trafficking (Godena et al., 2014). However, our data suggest that the altered mitochondrial trafficking may be independent of mutant *LRRK2* as neither *LRRK2* G2019S-expressing glutamatergic neurons nor sensory neurons exhibit altered mitochondrial trafficking, and the *LRRK2* kinase inhibitor GSK2578215A did not improve trafficking defects in dopaminergic neurons. It is important to note that our data are in contrast to a recent report showing that NAD⁺ levels and SIRT2 deacetylase activity were increased in PD patient-derived hybrid cell lines (Esteves et al., 2017). This discrepancy could be due to differences between the hybrid and iPSC model systems, but another plausible explanation could be due to variations in NAD⁺ levels among different cell types, as demonstrated by the variable levels in dopaminergic, glutamatergic, and sensory neurons.

As the main mitochondrial deacetylase, SIRT3 has also been shown to regulate many aspects of mitochondrial function, including metabolism, ATP generation, and limiting oxidative stress (Shi et al., 2005; Hallows et al., 2006; Lombard et al., 2007). Mechanistically, SIRT3 has been directly linked to reducing ROS production through activation of SOD2 (Qiu et al., 2010; Someya et al., 2010; Tao et al., 2010). In PD, SIRT3 has been implicated as a causative factor in dopaminergic neuron loss in MPTP- and rotenone-treated neurons (Zhang et al., 2016a, 2016b). Although we observe increased SIRT3 protein levels in *LRRK2* G2019S iPSC-derived dopaminergic neurons, as



was the case for SIRT1 and SIRT2, increased expression did not correlate with increased activity, which is likely due to lower NAD⁺ levels in *LRRK2* G2019S iPSC-derived dopaminergic cultures.

Our data demonstrate unique, and potentially *LRRK2* kinase-independent, changes in sirtuin activity and NAD⁺ levels in human dopaminergic neurons expressing the *LRRK2* G2019S PD-associated mutation and may underlie pathological mechanisms of dopaminergic neuron loss in PD. The results of these studies also provide further insight into the role of sirtuins in dopaminergic neurons and stress the importance of considering NAD⁺ levels in conjunction with sirtuin activity when designing therapeutic intervention for the treatment of PD.

EXPERIMENTAL PROCEDURES

Cell Culture

Human iPSCs were obtained from publically available samples derived from two homozygous *LRRK2* G2019S patients (ND35367**C*, ND40018**C* Coriell Institute) and one heterozygous *LRRK2* G2019S patient (ND40019**C* Coriell Institute). Three previously characterized unaffected control lines were used (GM003814 Coriell Institute, GM02183 Coriell Institute, iPSC3; [Ebert et al., 2009](#); [Si-Tayeb et al., 2010](#); [HD iPSC Consortium, 2012](#)). A table describing the demographic, reprogramming, and source information for the control and PD iPSC lines is provided in our previously published work ([Schwab and Ebert, 2015](#)). Karyotypically normal iPSCs, used between passages 5 and 10, were grown in feeder-free conditions on Matrigel substrate in StemMACS iPS-Brew (Miltenyi). Karyotype G-banding was performed by Cell Line Genetics (Madison, WI). Neural progenitor cells (EZ spheres) were generated and maintained as described previously ([Ebert et al., 2013](#)). The use of iPSCs was approved by the Medical College of Wisconsin's Institutional Review Board (PRO25822) and the Human Stem Cell Research Oversight Committee.

Neural Differentiation

EZ spheres were differentiated into dopaminergic neurons using fibroblast growth factor-8, purmorphamine, and growth factors as described previously ([Ebert et al., 2013](#)). Telencephalic excitatory projection neurons were derived from EZ spheres as described previously ([Ebert et al., 2013](#)). Sensory neurons were derived from monolayer iPSCs as described previously ([Chambers et al., 2012](#)). For *LRRK2* kinase inhibition experiments, 1 μ M GSK2578215A (Tocris) was added at every feeding starting at 1 week prior to endpoint analysis. DMSO (1 μ M) was used as the vehicle control. All analyses were performed at 5 weeks of total differentiation for dopaminergic neurons and 4 weeks of total differentiation for glutamatergic and sensory neurons.

Immunocytochemistry

Plated cells were fixed in 4% paraformaldehyde in PBS (pH 7.4) for 20 min at room temperature. Nonspecific labeling was blocked and the cells permeabilized prior to primary antibody incubation. Cells

were subsequently labeled with the appropriate fluorescently tagged secondary antibodies. Hoechst nuclear dye was used to label nuclei. Antibodies are listed in [Table S1](#).

Western Blot

Whole-cell lysates were isolated from dopaminergic and glutamatergic neuron cultures using 1 \times 3-[(3-cholamidopropyl)dimethylammonio]-1-propanesulfonate (CHAPS) Cell Extract buffer with protease inhibitors (Cell Signaling Technology). Twenty micrograms of protein was run on 10% Tris-HCl polyacrylamide gels (Bio-Rad), transferred to polyvinylidene fluoride membrane (Millipore), and probed following standard chemiluminescent methods. Alternatively, membranes were probed following the LI-COR fluorescent western blot protocol and scanned using the Odyssey Infrared Imaging System. Protein quantifications were normalized using glyceraldehyde-3-phosphate dehydrogenase or REVERT Total Protein Stain. Antibodies are listed in [Table S1](#).

Mitochondrial Content and Distribution

Images were acquired from five random fields per coverslip and then analyzed using region of interest and line scan tools included in NIS Elements software. For region of interest measurements, the entire neuron was automatically traced and then TOM20 intensity was measured over this area. For line scan measurements, neurites projecting from a cell body were randomly selected and then measured for TOM20 intensity along the neurite length. Each neurite measurement was then divided into quartiles with respect to each neurite's overall length. A minimum of 250 neurons were analyzed from each line. Only TH⁺ (dopaminergic), TUJ1⁺ (glutamatergic), and peripherin⁺ (sensory neurons) were analyzed.

Mitochondrial Trafficking

Plated cells were loaded with 25 nM MitoTracker Green FM (Thermo Scientific; M7514) for 15 min, washed, and imaged on a Nikon fluorescent microscope. Videos were acquired from at least 5 random fields per coverslip, and a minimum of 250 neurons were analyzed and calculated using NIS Element kymograph software. Only the mitochondria found in neurites projecting from clearly identifiable cell bodies were used to determine anterograde and retrograde mitochondrial movement.

Mitochondrial Bioenergetics

iPSC lines were seeded onto Seahorse Bioscience 96-well microplates and patterned toward dopaminergic, glutamatergic, and sensory neurons. The plates were analyzed using a standard method for measuring OCR using the XFe96 Extracellular Flux Analyzer ([Dranka et al., 2011](#); [Patitucci and Ebert, 2016](#)).

Nucleotide Measurements

ATP, ADP, and NAD⁺ were analyzed by high-performance liquid chromatography (HPLC) following perchloric acid precipitation, as described previously ([Perez et al., 2010](#)). Solvent A (125 μ L; 0.1 M potassium phosphate and 4 mM tetrabutylammonium bisulfate [pH 6.0], diluted 64:36 in water [v/v]) was added to the supernatants (100 μ L). Protein concentrations were determined by Bradford assay using 1 \times CHAPS buffer with PMSF and 1 \times DTT



(Cell Signaling Technology). HPLC analysis of nucleotides was performed on a Supelco C-18 column using solvent A and solvent B (0.1 M potassium phosphate and 4 mM tetrabutylammonium bisulfate [pH 6.0], diluted 64:36 in methanol [v/v]) with a flow rate of 1 mL/min. The column was equilibrated with solvent A, and the compounds were eluted during a linear increase in the level of solvent B to 50% between 1.5 and 5.5 min, followed by an increase to 65% over the next 7.5 min. ATP, ADP, and NAD⁺ peaks were measured for each sample, compared with the standards, and expressed in nmol per mg of protein.

Statistical Analysis

Data are from a minimum of three independent experiments, each with a minimum of three biological replicates. Samples were blinded prior to analysis. With consultation from the Department of Biostatistics at the Medical College of Wisconsin, statistical analysis was performed with GraphPad Prism software using one-way ANOVA, one-way repeated measures ANOVA, or two-way repeated measures ANOVA with Tukey *post-hoc* analysis. Results are presented as mean ± SEM and considered statistically significant at $p < 0.05$.

SUPPLEMENTAL INFORMATION

Supplemental Information includes six figures and one table and can be found with this article online at <https://doi.org/10.1016/j.stemcr.2017.10.010>.

AUTHOR CONTRIBUTIONS

Conception and Design, A.J.S. and A.D.E.; Collection and/or Assembly of Data, A.J.S., S.L.S., M.R.M., K.A.B., and A.D.E.; Data Analysis and Interpretation, A.J.S., S.L.S., K.A.B., and A.D.E.; Provision of Study Materials, J.A.C. and A.D.E.; Manuscript Writing and/or Editing, A.J.S., S.L.S., K.A.B., J.A.C., and A.D.E. All authors provided input for the final submitted manuscript.

ACKNOWLEDGMENTS

The authors thank the Department of Biostatistics at the Medical College of Wisconsin (MCW) for consultation services and Steve Komars for assistance with the Seahorse Bioanalyzer. This project was funded in part by the Imagine More Award from the Neuroscience Research Center at MCW (to A.D.E.), Advancing a Healthier Wisconsin (to A.D.E.), the Fraternal Order of Eagles (to A.D.E.), and the NIH DK052194 (to J.A.C.), AI044458 (to J.A.C.), P30DK020595 (to K.A.B.), and 2T35AG29793 (to M.R.M.). The content is solely the responsibility of the authors and does not necessarily represent the official views of the NIH.

Received: March 28, 2017

Revised: October 10, 2017

Accepted: October 11, 2017

Published: November 9, 2017

REFERENCES

Ashrafi, G., and Schwarz, T.L. (2013). The pathways of mitophagy for quality control and clearance of mitochondria. *Cell Death Differ.* 20, 31–42.

Buler, M., Andersson, U., and Hakkola, J. (2016). Who watches the watchmen? Regulation of the expression and activity of sirtuins. *FASEB J.* 30, 3942–3960.

Canto, C., Gerhart-Hines, Z., Feige, J.N., Lagouge, M., Noriega, L., Milne, J.C., Elliott, P.J., Puigserver, P., and Auwerx, J. (2009). AMPK regulates energy expenditure by modulating NAD⁺ metabolism and SIRT1 activity. *Nature* 458, 1056–1060.

Chalkiadaki, A., and Guarente, L. (2012). Sirtuins mediate mammalian metabolic responses to nutrient availability. *Nat. Rev. Endocrinol.* 8, 287–296.

Chambers, S.M., Fasano, C.A., Papapetrou, E.P., Tomishima, M., Sadelain, M., and Studer, L. (2009). Highly efficient neural conversion of human ES and iPS cells by dual inhibition of SMAD signaling. *Nat. Biotechnol.* 27, 275–280.

Chambers, S.M., Qi, Y., Mica, Y., Lee, G., Zhang, X.J., Niu, L., Bilsland, J., Cao, L., Stevens, E., Whiting, P., et al. (2012). Combined small-molecule inhibition accelerates developmental timing and converts human pluripotent stem cells into nociceptors. *Nat. Biotechnol.* 30, 715–720.

Chen, S., Owens, G.C., Makarenkova, H., and Edelman, D.B. (2010). HDAC6 regulates mitochondrial transport in hippocampal neurons. *PLoS One* 5, e10848.

Chen, X., Wales, P., Quinti, L., Zuo, F., Moniot, S., Herisson, F., Rauf, N.A., Wang, H., Silverman, R.B., Ayata, C., et al. (2015). The sirtuin-2 inhibitor AK7 is neuroprotective in models of Parkinson's disease but not amyotrophic lateral sclerosis and cerebral ischemia. *PLoS One* 10, e0116919.

Cherra, S.J., 3rd, Kulich, S.M., Uechi, G., Balasubramani, M., Mountzouris, J., Day, B.W., and Chu, C.T. (2010). Regulation of the autophagy protein LC3 by phosphorylation. *J. Cell Biol.* 190, 533–539.

Cherra, S.J., 3rd, Steer, E., Gusdon, A.M., Kiselyov, K., and Chu, C.T. (2013). Mutant LRRK2 elicits calcium imbalance and depletion of dendritic mitochondria in neurons. *Am. J. Pathol.* 182, 474–484.

Cooper, O., Seo, H., Andrabi, S., Guardia-Laguarta, C., Graziotto, J., Sundberg, M., McLean, J.R., Carrillo-Reid, L., Xie, Z., Osborn, T., et al. (2012). Pharmacological rescue of mitochondrial deficits in iPSC-derived neural cells from patients with familial Parkinson's disease. *Sci. Transl. Med.* 4, 141ra190.

Cronin-Furman, E.N., Borland, M.K., Bergquist, K.E., Bennett, J.P., Jr., and Trimmer, P.A. (2013). Mitochondrial quality, dynamics and functional capacity in Parkinson's disease cybrid cell lines selected for Lewy body expression. *Mol. Neurodegener.* 8, 6.

Di Fruscia, P., Zacharioudakis, E., Liu, C., Moniot, S., Laohasinnarong, S., Khongkow, M., Harrison, I.F., Koltsida, K., Reynolds, C.R., Schmidtkunz, K., et al. (2015). The discovery of a highly selective 5,6,7,8-tetrahydrobenzo[4,5]thieno[2,3-d]pyrimidin-4(3H)-one SIRT2 inhibitor that is neuroprotective in an in vitro Parkinson's disease model. *Chem. Med. Chem.* 10, 69–82.

Dranka, B.P., Benavides, G.A., Diers, A.R., Giordano, S., Zelickson, B.R., Reily, C., Zou, L., Chatham, J.C., Hill, B.G., Zhang, J., et al. (2011). Assessing bioenergetic function in response to oxidative stress by metabolic profiling. *Free Radic. Biol. Med.* 51, 1621–1635.



- Ebert, A.D., Yu, J., Rose, F.F., Jr., Mattis, V.B., Lorson, C.L., Thomson, J.A., and Svendsen, C.N. (2009). Induced pluripotent stem cells from a spinal muscular atrophy patient. *Nature* 457, 277–280.
- Ebert, A.D., Shelley, B.C., Hurley, A.M., Onorati, M., Castiglioni, V., Patitucci, T.N., Svendsen, S.P., Mattis, V.B., McGivern, J.V., Schwab, A.J., et al. (2013). EZ spheres: a stable and expandable culture system for the generation of pre-rosette multipotent stem cells from human ESCs and iPSCs. *Stem Cell Res.* 10, 417–427.
- Esteves, A.R., Gozes, I., and Cardoso, S.M. (2014). The rescue of microtubule-dependent traffic recovers mitochondrial function in Parkinson's disease. *Biochim. Biophys. Acta* 1842, 7–21.
- Esteves, A.R., Arduino, D.M., Silva, D.F., Viana, S.D., Pereira, F.C., and Cardoso, S.M. (2017). Mitochondrial metabolism regulates microtubule acetylation and autophagy through sirtuin-2: impact for Parkinson's disease. *Mol. Neurobiol.* <https://doi.org/10.1007/s12035-017-0420-y>.
- Gatto, E.M., Parisi, V., Converso, D.P., Poderoso, J.J., Carreras, M.C., Marti-Masso, J.F., and Paisan-Ruiz, C. (2013). The LRRK2 G2019S mutation in a series of Argentinean patients with Parkinson's disease: clinical and demographic characteristics. *Neurosci. Lett.* 537, 1–5.
- Godena, V.K., Brookes-Hocking, N., Moller, A., Shaw, G., Oswald, M., Sancho, R.M., Miller, C.C., Whitworth, A.J., and De Vos, K.J. (2014). Increasing microtubule acetylation rescues axonal transport and locomotor deficits caused by LRRK2 Roc-COR domain mutations. *Nat. Commun.* 5, 5245.
- Greggio, E., Jain, S., Kingsbury, A., Bandopadhyay, R., Lewis, P., Kaganovich, A., van der Brug, M.P., Beilina, A., Blackinton, J., Thomas, K.J., et al. (2006). Kinase activity is required for the toxic effects of mutant LRRK2/dardarin. *Neurobiol. Dis.* 23, 329–341.
- Guarente, L. (2013). Calorie restriction and sirtuins revisited. *Genes Dev.* 27, 2072–2085.
- Hallows, W.C., Lee, S., and Denu, J.M. (2006). Sirtuins deacetylate and activate mammalian acetyl-CoA synthetases. *Proc. Natl. Acad. Sci. USA* 103, 10230–10235.
- HD iPSC Consortium (2012). Induced pluripotent stem cells from patients with Huntington's disease show CAG repeat expansion-associated phenotypes. *Cell Stem Cell* 11, 264–278.
- Herskovits, A.Z., and Guarente, L. (2013). Sirtuin deacetylases in neurodegenerative diseases of aging. *Cell Res.* 23, 746–758.
- Jaleel, M., Nichols, R.J., Deak, M., Campbell, D.G., Gillardon, F., Knebel, A., and Alessi, D.R. (2007). LRRK2 phosphorylates moesin at threonine-558: characterization of how Parkinson's disease mutants affect kinase activity. *Biochem. J.* 405, 307–317.
- Kang, J.S., Tian, J.H., Pan, P.Y., Zald, P., Li, C., Deng, C., and Sheng, Z.H. (2008). Docking of axonal mitochondria by syntaphilin controls their mobility and affects short-term facilitation. *Cell* 132, 137–148.
- Kim, D.S., Ross, P.J., Zaslavsky, K., and Ellis, J. (2014). Optimizing neuronal differentiation from induced pluripotent stem cells to model ASD. *Front. Cell. Neurosci.* 8, 109.
- Kriks, S., Shim, J.W., Piao, J., Ganat, Y.M., Wakeman, D.R., Xie, Z., Carrillo-Reid, L., Auyeung, G., Antonacci, C., Buch, A., et al. (2011). Dopamine neurons derived from human ES cells efficiently engraft in animal models of Parkinson's disease. *Nature* 480, 547–551.
- Liu, L., Arun, A., Ellis, L., Peritore, C., and Donmez, G. (2014). SIRT2 enhances 1-methyl-4-phenyl-1,2,3,6-tetrahydropyridine (MPTP)-induced nigrostriatal damage via apoptotic pathway. *Front. Aging Neurosci.* 6, 184.
- Liu, Z., Wang, X., Yu, Y., Li, X., Wang, T., Jiang, H., Ren, Q., Jiao, Y., Sawa, A., Moran, T., et al. (2008). A *Drosophila* model for LRRK2-linked parkinsonism. *Proc. Natl. Acad. Sci. USA* 105, 2693–2698.
- Lombard, D.B., Alt, F.W., Cheng, H.L., Bunkenborg, J., Streeper, R.S., Mostoslavsky, R., Kim, J., Yancopoulos, G., Valenzuela, D., Murphy, A., et al. (2007). Mammalian Sir2 homolog SIRT3 regulates global mitochondrial lysine acetylation. *Mol. Cell. Biol.* 27, 8807–8814.
- Luzon-Toro, B., Rubio de la Torre, E., Delgado, A., Perez-Tur, J., and Hilfiker, S. (2007). Mechanistic insight into the dominant mode of the Parkinson's disease-associated G2019S LRRK2 mutation. *Hum. Mol. Genet.* 16, 2031–2039.
- MacLeod, D., Dowman, J., Hammond, R., Leete, T., Inoue, K., and Abeliovich, A. (2006). The familial Parkinsonism gene LRRK2 regulates neurite process morphology. *Neuron* 52, 587–593.
- Makela, J., Mudo, G., Pham, D.D., Di Liberto, V., Eriksson, O., Louhivuori, L., Bruelle, C., Soliymani, R., Baumann, M., Korhonen, L., et al. (2016). Peroxisome proliferator-activated receptor-gamma coactivator-1alpha mediates neuroprotection against excitotoxic brain injury in transgenic mice: role of mitochondria and X-linked inhibitor of apoptosis protein. *Eur. J. Neurosci.* 43, 626–639.
- Mariani, J., Simonini, M.V., Palejev, D., Tomasini, L., Coppola, G., Szekely, A.M., Horvath, T.L., and Vaccarino, F.M. (2012). Modeling human cortical development in vitro using induced pluripotent stem cells. *Proc. Natl. Acad. Sci. USA* 109, 12770–12775.
- Mortiboys, H., Furmston, R., Bronstad, G., Aasly, J., Elliott, C., and Bandmann, O. (2015). UDCA exerts beneficial effect on mitochondrial dysfunction in LRRK2(G2019S) carriers and in vivo. *Neurology* 85, 846–852.
- Mortiboys, H., Johansen, K.K., Aasly, J.O., and Bandmann, O. (2010). Mitochondrial impairment in patients with Parkinson disease with the G2019S mutation in LRRK2. *Neurology* 75, 2017–2020.
- Ng, C.H., Mok, S.Z., Koh, C., Ouyang, X., Fivaz, M.L., Tan, E.K., Dawson, V.L., Dawson, T.M., Yu, F., and Lim, K.L. (2009). Parkin protects against LRRK2 G2019S mutant-induced dopaminergic neurodegeneration in *Drosophila*. *J. Neurosci.* 29, 11257–11262.
- Nguyen, H.N., Byers, B., Cord, B., Shcheglovitov, A., Byrne, J., Gujar, P., Kee, K., Schule, B., Dolmetsch, R.E., Langston, W., et al. (2011). LRRK2 mutant iPSC-derived DA neurons demonstrate increased susceptibility to oxidative stress. *Cell Stem Cell* 8, 267–280.
- North, B.J., Marshall, B.L., Borra, M.T., Denu, J.M., and Verdin, E. (2003). The human Sir2 ortholog, SIRT2, is an NAD⁺-dependent tubulin deacetylase. *Mol. Cell* 11, 437–444.
- Outeiro, T.F., Kontopoulos, E., Altmann, S.M., Kufareva, I., Strathearn, K.E., Amore, A.M., Volk, C.B., Maxwell, M.M., Rochet, J.C., McLean, P.J., et al. (2007). Sirtuin 2 inhibitors rescue alpha-synuclein-mediated toxicity in models of Parkinson's disease. *Science* 317, 516–519.



- Papkovskaia, T.D., Chau, K.Y., Inesta-Vaquera, F., Papkovsky, D.B., Healy, D.G., Nishio, K., Staddon, J., Duchen, M.R., Hardy, J., Schapira, A.H., et al. (2012). G2019S leucine-rich repeat kinase 2 causes uncoupling protein-mediated mitochondrial depolarization. *Hum. Mol. Genet.* *21*, 4201–4213.
- Patel, V.P., and Chu, C.T. (2014). Decreased SIRT2 activity leads to altered microtubule dynamics in oxidatively-stressed neuronal cells: implications for Parkinson's disease. *Exp. Neurol.* *257*, 170–181.
- Patitucci, T.N., and Ebert, A.D. (2016). SMN deficiency does not induce oxidative stress in SMA iPSC-derived astrocytes or motor neurons. *Hum. Mol. Genet.* *25*, 514–523.
- Perez, J., Hill, B.G., Benavides, G.A., Dranka, B.P., and Darley-Usmar, V.M. (2010). Role of cellular bioenergetics in smooth muscle cell proliferation induced by platelet-derived growth factor. *Biochem. J.* *428*, 255–267.
- Plowey, E.D., Cherra, S.J., 3rd, Liu, Y.J., and Chu, C.T. (2008). Role of autophagy in G2019S-LRRK2-associated neurite shortening in differentiated SH-SY5Y cells. *J. Neurochem.* *105*, 1048–1056.
- Qiu, X., Brown, K., Hirschey, M.D., Verdin, E., and Chen, D. (2010). Calorie restriction reduces oxidative stress by SIRT3-mediated SOD2 activation. *Cell Metab.* *12*, 662–667.
- Ramonet, D., Daher, J.P., Lin, B.M., Stafa, K., Kim, J., Banerjee, R., Westerlund, M., Pletnikova, O., Glauser, L., Yang, L., et al. (2011). Dopaminergic neuronal loss, reduced neurite complexity and autophagic abnormalities in transgenic mice expressing G2019S mutant LRRK2. *PLoS One* *6*, e18568.
- Reinhardt, P., Schmid, B., Burbulla, L.F., Schondorf, D.C., Wagner, L., Glatza, M., Hoing, S., Hargus, G., Heck, S.A., Dhingra, A., et al. (2013). Genetic correction of a LRRK2 mutation in human iPSCs links parkinsonian neurodegeneration to ERK-dependent changes in gene expression. *Cell Stem Cell* *12*, 354–367.
- Reith, A.D., Bamborough, P., Jandu, K., Andreotti, D., Mensah, L., Dossang, P., Choi, H.G., Deng, X., Zhang, J., Alessi, D.R., et al. (2012). GSK2578215A; a potent and highly selective 2-arylmethoxy-5-substituent-N-arylbenzamide LRRK2 kinase inhibitor. *Bioorg. Med. Chem. Lett.* *22*, 5625–5629.
- Revollo, J.R., and Li, X. (2013). The ways and means that fine tune Sirt1 activity. *Trends Biochem. Sci.* *38*, 160–167.
- Rodgers, J.T., Lerin, C., Haas, W., Gygi, S.P., Spiegelman, B.M., and Puigserver, P. (2005). Nutrient control of glucose homeostasis through a complex of PGC-1alpha and SIRT1. *Nature* *434*, 113–118.
- Ryan, B.J., Hoek, S., Fon, E.A., and Wade-Martins, R. (2015). Mitochondrial dysfunction and mitophagy in Parkinson's: from familial to sporadic disease. *Trends Biochem. Sci.* *40*, 200–210.
- Saha, S., Guillily, M.D., Ferree, A., Lanceta, J., Chan, D., Ghosh, J., Hsu, C.H., Segal, L., Raghavan, K., Matsumoto, K., et al. (2009). LRRK2 modulates vulnerability to mitochondrial dysfunction in *Caenorhabditis elegans*. *J. Neurosci.* *29*, 9210–9218.
- Sanchez-Danes, A., Richaud-Patin, Y., Carballo-Carbajal, I., Jimenez-Delgado, S., Caig, C., Mora, S., Di Guglielmo, C., Ezquerro, M., Patel, B., Giralt, A., et al. (2012). Disease-specific phenotypes in dopamine neurons from human iPSC-based models of genetic and sporadic Parkinson's disease. *EMBO Mol. Med.* *4*, 380–395.
- Sanders, L.H., Laganier, J., Cooper, O., Mak, S.K., Vu, B.J., Huang, Y.A., Paschon, D.E., Vangipuram, M., Sundararajan, R., Urnov, F.D., et al. (2014). LRRK2 mutations cause mitochondrial DNA damage in iPSC-derived neural cells from Parkinson's disease patients: reversal by gene correction. *Neurobiol. Dis.* *62*, 381–386.
- Schwab, A.J., and Ebert, A.D. (2015). Neurite aggregation and calcium dysfunction in iPSC-derived sensory neurons with Parkinson's disease-related LRRK2 G2019S mutation. *Stem Cell Reports* *5*, 1039–1052.
- Schwarz, T.L. (2013). Mitochondrial trafficking in neurons. *Cold Spring Harb. Perspect. Biol.* *5*. <https://doi.org/10.1101/cshperspect.a011304>.
- Shi, T., Wang, F., Stieren, E., and Tong, Q. (2005). SIRT3, a mitochondrial sirtuin deacetylase, regulates mitochondrial function and thermogenesis in brown adipocytes. *J. Biol. Chem.* *280*, 13560–13567.
- Shi, Y., Kirwan, P., Smith, J., Robinson, H.P., and Livesey, F.J. (2012). Human cerebral cortex development from pluripotent stem cells to functional excitatory synapses. *Nat. Neurosci.* *15*, 477–486.
- Si-Tayeb, K., Noto, F.K., Sepac, A., Sedlic, F., Bosnjak, Z.J., Lough, J.W., and Duncan, S.A. (2010). Generation of human induced pluripotent stem cells by simple transient transfection of plasmid DNA encoding reprogramming factors. *BMC Dev. Biol.* *10*, 81.
- Someya, S., Yu, W., Hallows, W.C., Xu, J., Vann, J.M., Leeuwenburgh, C., Tanokura, M., Denu, J.M., and Prolla, T.A. (2010). Sirt3 mediates reduction of oxidative damage and prevention of age-related hearing loss under caloric restriction. *Cell* *143*, 802–812.
- Tang, B.L. (2017). Sirtuins as modifiers of Parkinson's disease pathology. *J. Neurosci. Res.* *95*, 930–942.
- Tao, R., Coleman, M.C., Pennington, J.D., Ozden, O., Park, S.H., Jiang, H., Kim, H.S., Flynn, C.R., Hill, S., Hayes McDonald, W., et al. (2010). Sirt3-mediated deacetylation of evolutionarily conserved lysine 122 regulates MnSOD activity in response to stress. *Mol. Cell* *40*, 893–904.
- Wang, D., Tang, B., Zhao, G., Pan, Q., Xia, K., Bodmer, R., and Zhang, Z. (2008). Dispensable role of *Drosophila* ortholog of LRRK2 kinase activity in survival of dopaminergic neurons. *Mol. Neurodegener.* *3*, 3.
- Weir, H.J., Lane, J.D., and Balthasar, N. (2013). SIRT3: a central regulator of mitochondrial adaptation in health and disease. *Genes Cancer* *4*, 118–124.
- West, A.B., Moore, D.J., Biskup, S., Bugayenko, A., Smith, W.W., Ross, C.A., Dawson, V.L., and Dawson, T.M. (2005). Parkinson's disease-associated mutations in leucine-rich repeat kinase 2 augment kinase activity. *Proc. Natl. Acad. Sci. USA* *102*, 16842–16847.
- Wilson, B.J., Tremblay, A.M., Deblois, G., Sylvain-Drolet, G., and Giguere, V. (2010). An acetylation switch modulates the transcriptional activity of estrogen-related receptor alpha. *Mol. Endocrinol.* *24*, 1349–1358.
- Yamaguchi, H., Woods, N.T., Piluso, L.G., Lee, H.H., Chen, J., Bhalla, K.N., Monteiro, A., Liu, X., Hung, M.C., and Wang, H.G.



- (2009). p53 acetylation is crucial for its transcription-independent proapoptotic functions. *J. Biol. Chem.* *284*, 11171–11183.
- Yue, M., Hinkle, K.M., Davies, P., Trushina, E., Fiesel, F.C., Christenson, T.A., Schroeder, A.S., Zhang, L., Bowles, E., Behrouz, B., et al. (2015). Progressive dopaminergic alterations and mitochondrial abnormalities in LRRK2 G2019S knock-in mice. *Neurobiol. Dis.* *78*, 172–195.
- Zhang, J., Nuebel, E., Wisidagama, D.R., Setoguchi, K., Hong, J.S., Van Horn, C.M., Imam, S.S., Vergnes, L., Malone, C.S., Koehler, C.M., et al. (2012). Measuring energy metabolism in cultured cells, including human pluripotent stem cells and differentiated cells. *Nat. Protoc.* *7*, 1068–1085.
- Zhang, J.Y., Deng, Y.N., Zhang, M., Su, H., and Qu, Q.M. (2016a). SIRT3 acts as a neuroprotective agent in rotenone-induced Parkinson cell model. *Neurochem. Res.* *41*, 1761–1773.
- Zhang, X., Ren, X., Zhang, Q., Li, Z., Ma, S., Bao, J., Bai, X., Zheng, L., Zhang, Z., Shang, S., et al. (2016b). PGC-1alpha/ERRalpha-Sirt3 pathway regulates DAergic neuronal death by directly deacetylating SOD2 and ATP synthase beta. *Antioxid. Redox Signal.* *24*, 312–328.